JMB

Available online at www.sciencedirect.com

ScienceDirect

ELSEVIER

Two Amyloid States of the Prion Protein Display Significantly Different Folding Patterns

Valeriy G. Ostapchenko[1], Michael R. Sawaya[2], Natallia Makarava[1], Regina Savtchenko[1], K. Peter R. Nilsson[3], David Eisenberg[2] and Ilia V. Baskakov[1,4]*

[1]*Center for Biomedical Engineering and Technology, University of Maryland, Baltimore, MD 21201, USA*

[2]*Howard Hughes Medical Institute, UCLA-DOE Institute for Genomics and Proteomics, Los Angeles, CA 90095-1570, USA*

[3]*Department of Chemistry, Linkoping University, Linkoping, Sweden*

[4]*Department of Biochemistry and Molecular Biology, University of Maryland, Baltimore, MD 21201, USA*

It has been well established that a single amino acid sequence can give rise to several conformationally distinct amyloid states. The extent to which amyloid structures formed within the same sequence are different, however, remains unclear. To address this question, we studied two amyloid states (referred to as R- and S-fibrils) produced *in vitro* from highly purified full-length recombinant prion protein. Several biophysical techniques including X-ray diffraction, CD, Fourier transform infrared spectroscopy (FTIR), hydrogen–deuterium exchange, proteinase K digestion, and binding of a conformation-sensitive fluorescence dye revealed that R- and S-fibrils have substantially different secondary, tertiary, and quaternary structures. While both states displayed a 4. 8-Å meridional X-ray diffraction typical for amyloid cross-β-spines, they showed markedly different equatorial profiles, suggesting different folding pattern of β-strands. The experiments on hydrogen–deuterium exchange monitored by FTIR revealed that only small fractions of amide protons were protected in R- or S-fibrils, an argument for the dynamic nature of their cross-β-structure. Despite this fact, both amyloid states were found to be very stable conformationally as judged from temperature-induced denaturation monitored by FTIR and the conformation-sensitive dye. Upon heating to 80 °C, only local unfolding was revealed, while individual state-specific cross-β features were preserved. The current studies demonstrated that the two amyloid states formed by the same amino acid sequence exhibited significantly different folding patterns that presumably reflect two different architectures of cross-β-structure. Both S- and R-fibrils, however, shared high conformational stability, arguing that the energy landscape for protein folding and aggregation can contain several deep free-energy minima.

© 2010 Elsevier Ltd. All rights reserved.

Keywords: amyloid fibrils; prion protein; X-ray diffraction; FTIR; hydrogen–deuterium exchange

Edited by J. Weissman

---

*Corresponding author. E-mail address: Baskakov@umaryland.edu.

Introduction

It has been well established that conformationally different amyloid states can be produced by the same amino acid sequence.[1–5] The principle underlying the ability of a protein to acquire multiple self-propagating structures was first introduced by the protein-only hypothesis of prion propagation to explain formation of multiple prion strains within the same host.[6] While in the past this principle was considered to be limited to the mammalian prion protein, the ability of the same sequence to give rise to different self-propagating states has now been

well demonstrated for several yeast prion proteins and a number of disease-related or disease non-related polypeptides.[1,3–5,7–9]

The extent to which amyloid structures formed by the same sequence are different, however, is currently unclear. It is not known whether the state-specific variations in amyloid structures originate from fundamentally different global folds or only from minor variations within the same folding and assembly pattern. This question has numerous implications for our understanding of the origin of prion strains, the range of their biological activities, the conformational diversity of functional and pathological amyloids, and the mechanisms for protein-encoded inheritance.

To date, the mechanisms underlying the conformational differences in amyloid fibrils have been largely explored using relatively short peptides.[5,10,11] In recent studies, packing polymorphism (i.e., alternative packing arrangements of β-sheets formed by the same segment of a protein) and segmental polymorphism (i.e., different segments of a protein form β-sheets) were found to contribute to the structural diversity in amyloid fibrils formed by several hexapeptides.[5] Variations in symmetry of lateral interactions between protofilaments offer an additional source for structural polymorphism in amyloid fibrils.[10,12] Two amyloid states produced from Aβ(1–40) peptide were shown to consist of nearly identical β-strand segments that acquired either 2- and 3-fold symmetries when assembled into mature fibrils.[10]

Due to a number of technical difficulties, few studies have been undertaken to elucidate state-specific differences in amyloid fibrils produced by large polypeptides such as full-length prion protein. Because structural approaches are often limited to imaging techniques such as electron microscopy (EM) or atomic force microscopy (AFM), fibril morphology has been identified as one of the major tools for assessing structural polymorphism.[13–15] In addressing the question of state-specific structural differences, it is important to make a distinction between actual conformational polymorphisms that arise from different structures of cross β-spines and morphological polymorphisms that might occur solely as a result of alternative modes of lateral assembly of filaments. In previous studies, we showed that fibrils produced from the full-length recombinant prion protein (PrP) under a single set of growth conditions were highly polymorphous and that this polymorphism arises due to variations in the number of protofilaments and alternative modes of lateral assembly of protofilaments into mature fibrils.[16,17] Despite significant morphological polymorphism, however, the structure of the cross β-spine appeared to be uniform in these fibrils as judged from Fourier transform infrared spectroscopy (FTIR)[2] and hydrogen–deuterium (H/D) exchange Raman spectroscopy (I.V.B. and I. Lednev, unpublished observation). Surprisingly, prion strains isolated from scrapie brains were shown to display overlapping fibril morphologies.[18,19] Taken together, these results provide strong evidence that polymorphysm in fibril morphology does not directly report on state-specific or strain-specific cross-β-spine structures.

To test the extent to which amyloid states formed within the same primary structure are different, we used two types of amyloid fibrils (referred to as R- and S-fibrils) produced from highly purified full-length recombinant PrP.[2] Several biophysical techniques including X-ray diffraction, CD, FTIR, H/D exchange, proteinase K (PK) digestion, and binding of conformation-sensitive fluorescence dye revealed that two amyloid states exhibit significantly different folding patterns within their cross-β-sheet structure. X-ray diffraction analysis confirmed cross-β-structure for both states, but revealed radically different equatorial patterns. Remarkably, despite fundamental differences in global structures, both S- and R-fibrils were highly stable thermodynamically. Contrary to the commonly accepted view, this work suggests that the energy landscape for protein folding and assembly contains several global free-energy minima: one of which is occupied by a native state and more than one being occupied by amyloid states.

Results

Previously, we showed that two amyloid states referred to as R and S could be produced from full-length recombinant hamster PrP under two different agitation modes.[2] R- and S-fibrils displayed very distinctive morphologies as judged by EM and AFM (Supplementary Fig. 1). Considering that R- and S-fibrils were formed under identical solvent conditions from the same stock solution of PrP, we were interested in determining the extent to which their structures were different.

X-ray diffraction reports different folding patterns within cross-β-structures of R- and S-fibrils

Confirming that both states consist of cross-β-structure, X-ray diffraction analysis revealed a single major meridional reflection at 4.8 Å and equatorial reflections near 10 Å in both R- and S- fibrils (Fig. 1a). However, the two diffraction patterns were not identical; due to the relatively high degree of order in these fibrils, differences in the pattern of equatorial reflections were observed (Fig. 1b). The equatorial diffraction from R-fibrils showed 10-, 13.7-, 23-, and 44- Å bands, whereas S-fibrils displayed 7.3-, 9.3-, 10.9-, 15.3-, and 28.6- Å bands. These data suggest that the PrP molecules have distinct folding and assembly patterns within R- and S-fibrils.

R- and S-fibrils show substantial differences in their secondary structure

The infrared spectra of R- and S-fibrils were fitted using a combination of Gaussian peaks with
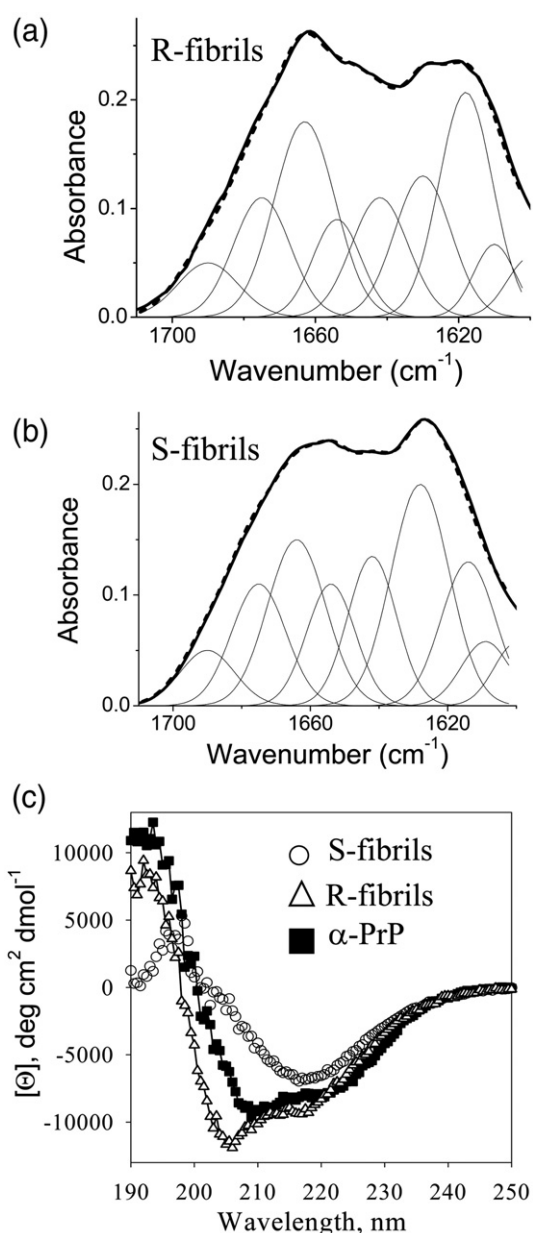
(a)

(b)
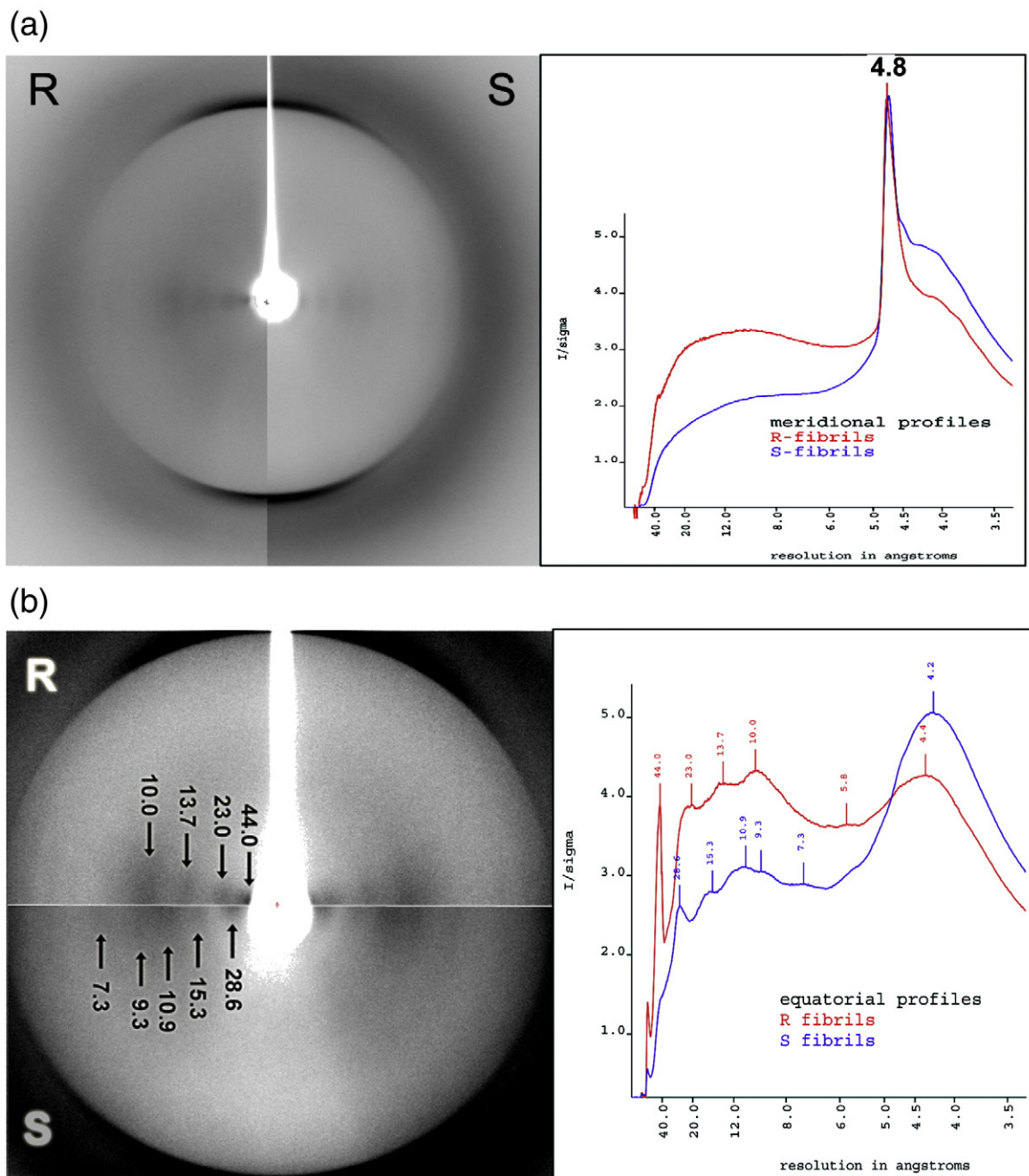
Fig. 1. X-ray diffraction of R- and S-fibrils. (a) Broad-range diffraction pattern displays a single 4.8-Å band in meridional profiles (vertical dissection) for both amyloid states. (b) Horizontal dissection (equatorial profile) of high-range diffraction pattern reveals distinctive sets of bands for R- and S-fibrils.

maxima taken from second derivatives of FTIR spectra to estimate the secondary-structure content (Fig. 2a and b). In our previous work, two FTIR bands corresponding to β-sheet structures were found for both R- and S-fibrils.[2] While the β-sheet component was predominant in both fibrillar types, the position and the ratio of two subcomponents were different in two amyloid states (Table 1). The subcomponents designated as CB-1 displayed maxima at 1630 and 1628 cm^{-1} for R- and S-fibrils, respectively, and the subcomponent CB-2 peaked at 1618 and 1614 cm^{-1} for R- and S-fibrils, respec-

tively. The peak at 1663 cm^{-1}, which is often assigned to turn conformations,[20] was more substantial in R- than in S-fibrils, suggesting that R-structure includes more β- or γ-turns. The percentage of unordered structure was the same in R- and S-fibrils (Table 1). In deconvoluting the FTIR spectra, it is important to keep in mind that due to uncertainty in width of the bands assigned to different elements of secondary structure, the estimation of secondary-structure content is subject to large errors.

CD spectroscopy confirmed significant differences in secondary structures between R- and S-fibrils.

S-fibrils showed spectra typical for β-sheet-rich proteins, whereas R-fibrils exhibited a substantial negative peak at 205 nm (Fig. 1c) that could be assigned to type I β-turns[21] and/or superhelical twists that are typical for R-fibril morphology (Supplementary Fig. 1). The latter explanation was supported by a decrease in the amplitude of the 205-nm peak that was observed upon intensive fragmentation of R-fibrils using sonication (Supplementary Fig. 2a). Therefore, the negative peak at 205 nm was attributed, in part, to superhelical twists

Table 1. Secondary-structure composition as determined from deconvolution and curve fitting of the FTIR amide I′ band

	Wavenumber (cm^{-1})	Secondary structure (%)[a]	
		R-fibrils	S-fibrils
α-Helix	~1654	9±3	11±3
Cross-β-sheet	CB-1[b]	16±1	26±2
	CB-2[c]	28.5±1.5	14.0±1.5
Turn conformations	~1663	21±2	15±1
	~1675	11±2	11±1
	~1690	4.2±0.7	4.5±0.3
Random coil	~1642	13±1	14±0.8

[a] Mean values±standard deviation for three independent preparations of PrP firbils.
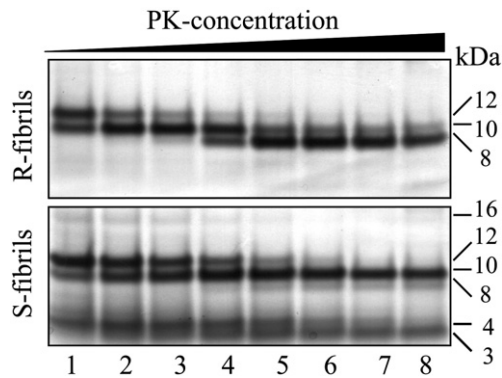[b] CB-1 band corresponds to 1630 or 1628 cm^{-1} for R- or S-fibrils, respectively.
[c] CB-2 band corresponds to 1618 or 1614 cm^{-1} for R- or S-fibrils, respectively.

witnessing left-handed helicity in R-fibrils. Nevertheless, even after sonication, significant differences remained between CD spectra of R- and S-fibrils. Both CD and FTIR spectroscopy revealed a substantially larger contribution of turn conformations in R-fibrils compared to that in S-fibrils.

N-terminal region is PK-resistant in S-fibrils

To determine whether the same PrP region is involved in forming the most proteolytically resistant cross-β-spine in two amyloid states, we employed a PK digestion assay. PK digestion followed by SDS-PAGE revealed a triplet of bands with molecular masses of 8, 10, and 12 kDa in both fibrillar types (Fig. 3). The relative intensity of bands, however, was markedly different for R- and S-fibrils. Upon increased PK concentration, R-fibrils showed a progressing reduction in the size of the PK-resistant spine from 12 to 10 kDa and finally to 8 kDa, whereas S-fibrils displayed a very stable spine of 10 kDa even at high PK concentrations. Furthermore, additional PK-resistant bands with apparent molecular masses of ~4 and 3 kDa were present in the digestion assays of S-fibrils. The 3-kDa band was as stable toward PK as the 10-kDa band. Amino acid sequencing by Edman revealed that the small PK-resistant products correspond to the very N-terminus of full-length PrP 23–231 starting from residue 23. Consistent with the sequencing results, none of the antibodies to the central or C-terminal PrP regions (to the epitopes 95–105, 108–111, 132–156, 160–170, or 224–230) were able to detect the short PK-resistant products on Western blotting (data not shown). In addition to the N-terminal peptides, S-fibrils consistently showed a minor 16-kDa band that was detectable only at lower concentrations of PK. The PK digestion assay illustrated that the cross-β-spine is likely to have a different folding pattern in the two amyloid states and that an additional region is involved in forming the fibrillar spine in S-fibrils. In S-fibrils, the N-terminal region was as stable to PK digestion as the

Fig. 2. Comparison of the secondary structure of R- and S-fibrils. The FTIR spectra (bold lines) and the results of curve fitting (broken lines) of the FTIR amide I′ region of R-fibrils (a) and S-fibrils (b). Peaks corresponding to individual components of secondary structure are shown by thin lines. (c) Far-UV CD spectra of S-fibrils (○), R-fibrils (△), and monomeric α-PrP (■).

Fig. 3. PK digestion assay of R-fibrils (top panel) and S-fibrils (bottom panel). PrP fibrils (100 μg/ml) were treated with PK for 1 h at 37 °C at the following concentrations (in micrograms per milliliter): 0.2 (lane 1), 0.5 (lane 2), 1 (lane 3), 2 (lane 4), 5 (lane 5), 10 (lane 6), 20 (lane 7), and 50 (lane 8) and analyzed by SDS-PAGE followed by silver staining. For R-fibrils, only three PK-resistant products of 12, 10, and 8 kDa, starting from the residues 138, 152 and 162, respectively, were found,[22] whereas S-fibrils showed additional PK-resistant products at 3 and 4 kDa.

C-terminal regions, illustrating that both regions are equally involved in forming the fibrillar spine.

H/D exchange showed higher amide protection in R- than in S-fibrils

A transition from the monomeric to the fibrillar state is known to result in a significant increase in amide protection, a process that can be assessed by H/D exchange combined with FTIR. To compare the level of amide protection in S- and R-fibrils, we employed two formats for H/D experiments: (i) PrP samples were dried and then dissolved in D_2O water prior to measurements ("dried samples") or (ii) PrP samples were concentrated in H_2O and then diluted with D_2O ("wet samples"). The H/D exchange rate was monitored by a shift of Amide II to Amide II' region in FTIR spectra (Fig. 4). Both types of fibrils showed very fast H/D exchange as judged by the disappearance of the Amide II peak within the first few minutes of experiment (Fig. 4a and b). R-fibrils, however, consistently showed a higher level of amide protection than S-fibrils in both experimental formats, as judged at the end time
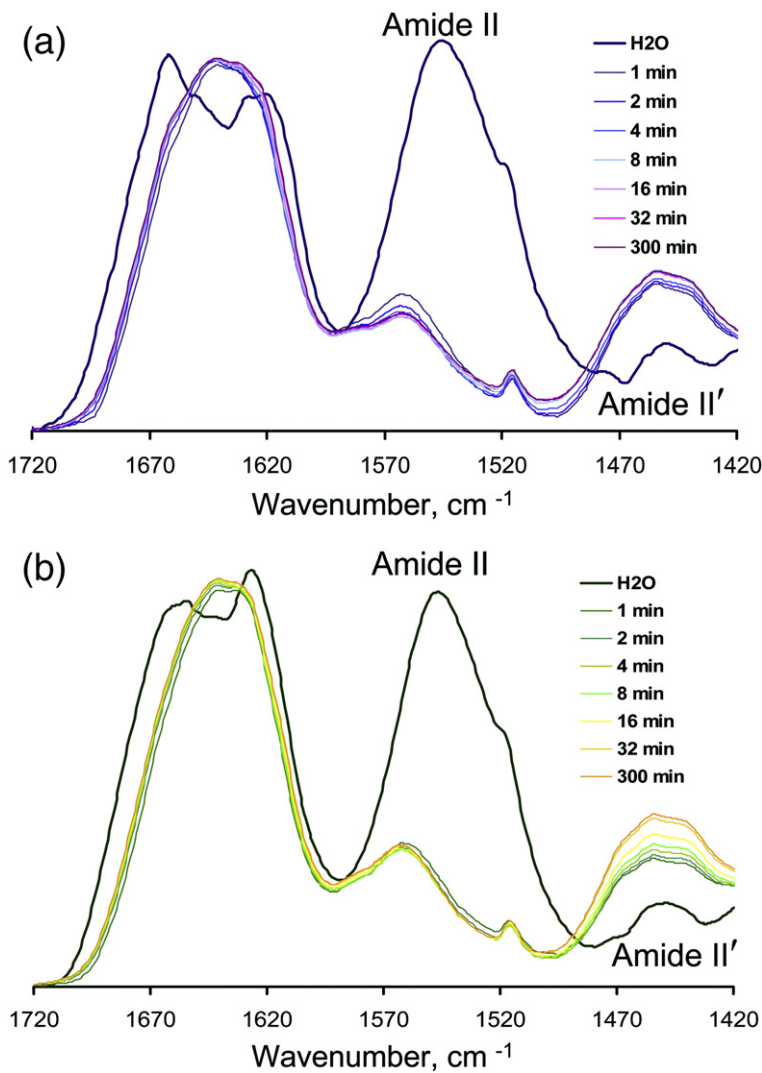
Fig. 4. H/D exchange of amide hydrogens in R-fibrils (a) and S-fibrils (b) as monitored by FTIR spectroscopy. PrP fibrils were dried using a Speed Vac, dissolved in D_2O, and FTIR spectra were collected at different time points over the following 5 h as indicated. FTIR spectra of fibrils in H_2O are shown by dark blue and dark green lines, for R- and S-fibrils, respectively.

point of the experiment (5 h of exchange) (Table 2). For instance, in "dried samples", R-fibrils displayed 24–28% protected amides, whereas only 14–20% of amides were protected in S-fibrils. For a set of globular proteins, the level of protection varied from 6.7% for α-PrP (recombinant prion protein refolded into monomeric α-helical conformation) to 13.5% for carbonic anhydrase (β-sheet-rich protein), reflecting the differences in secondary structure and in a fraction of intrinsically disordered regions between different proteins. In "wet samples", the level of amide protection was even less than those in "dried samples" for all three PrP isoforms (α-PrP and S- and R-fibrils) (Table 2). Aggregation of fibrils upon drying could account for higher values of amide protection in dried samples than in wet samples.

After replacing H_2O with D_2O, Amide I′ regions of the FTIR spectra showed immediate changes (Fig. 4). As judged from CD spectra, however, no alterations in secondary structures of R- or S-fibrils were observed upon replacing H_2O with D_2O (Supplementary Fig. 2b), arguing that the changes in FTIR spectra are attributable to the change of solvent.

Luminescent-conjugated polythiophene PTAA distinguishes R- and S-fibrils

Luminescent-conjugated polythiophenes (LCPs) including poly(thiophene-acetic acid) (PTAA) were previously shown to be effective in detecting conformational differences in amyloid fibrils and prion strains.[23,24] In the current study, the S-fibrils displayed a modest shift in the emission spectrum of PTAA relative to the spectrum of α-PrP monomer and showed an emission maximum at 582 nm (Fig. 5a). Binding of PTAA to the R-fibrils, however, caused much more substantial red shift in the emission maximum than the shift found for the S-fibrils (Fig. 5a). The same effect was observed using fluorescent microscopy where R-fibrils showed a higher ratio of red-to-green emission than the S-fibrils (Fig. 5b and c).

R- and S-fibrils preserve their individual state-specific features under partially denaturing conditions

To provide further insight into the question of whether state-specific conformations arise as a result of different global folding pattern or from the differences in local folds, we were interested in testing whether R- and S-fibrils preserve their individual features upon partial thermal denaturation. Analysis of PTAA fluorescence revealed that both R- and S-fibrils retained their state-specific emission profile upon heating to 80 °C and subsequent cooling (Fig. 6a and b). As judged from the second derivatives of FTIR spectra, heating to 80 °C caused significant changes in the ratio of CB-1 *versus* CB-2 peaks for R-fibrils and almost complete disappearance of the CB-2 subpeak in S-fibrils (Fig. 6c and d). However, even at 80 °C, both the

**Table 2.** Amide hydrogen protection in S-fibrils, R-fibrils, and globular proteins

	Conservation of amide hydrogen (%)[a]	
	Dried samples	Wet samples
α-PrP (monomer)	6.7	6.5
R-fibrils	28.4	14.1
	26.8	13.8
	24.1	16.2
S-fibrils	14.8	9.4
	17.6	8.2
	19.9	8.7
Alcohol dehydrogenase	6.9	n/a
Bovine serum albumin	8.8	n/a
Carbonic anhydrase	13.5	n/a

[a] Percentage of amide hydrogens that remained protected after 5 h of H/D exchange.

R- and S-fibrils preserved their individual FTIR signatures (two comparable peaks CB-1 and CB-2 corresponding to cross β-structure and the peak at 1663 cm^{-1} in R-fibrils; predominant CB-1 peak for S-fibrils). Remarkably, upon cooling, the temperature-induced changes in the secondary structure were completely reversible for R-fibrils and partially reversible for S-fibrils (Fig. 6e and f). These results strongly support the hypothesis that state-specific conformation originates from fundamentally different folding patterns and that both structures are conformationally very stable.

Discussion

The current study demonstrates that two amyloid states produced *in vitro* from full-length PrP had significantly different folding and assembly patterns. CD and FTIR spectroscopy revealed significant differences in secondary structure and specifically that the R-fibrils had substantially more populated turn conformations than the S-fibrils. X-ray diffraction showed that cross-β-structures were characterized by clearly different architecture. As judged from the proteolytic digestion, the PK-resistant spine consisted of the N-terminal and C-terminal regions in the S-fibrils but only the C-terminal region in the R-fibrils. The experiment on H/D exchange showed substantial differences between the levels of amide protection for these two fibrillar states. Interaction with a conformationally flexible fluorescent probe revealed striking differences in polypeptide packing. As judged from EM and AFM, R-fibrils consisted of multiple filaments and displayed a straight shape with complex twisted morphologies, whereas the S-fibrils were of a curvy shape and smooth morphology.[2] Taken together, our current and previous studies illustrate that R- and S-fibrils were different with respect to their secondary, tertiary, and quaternary structures and that the PrP polypeptide chain acquired different global assemblies in these two states.
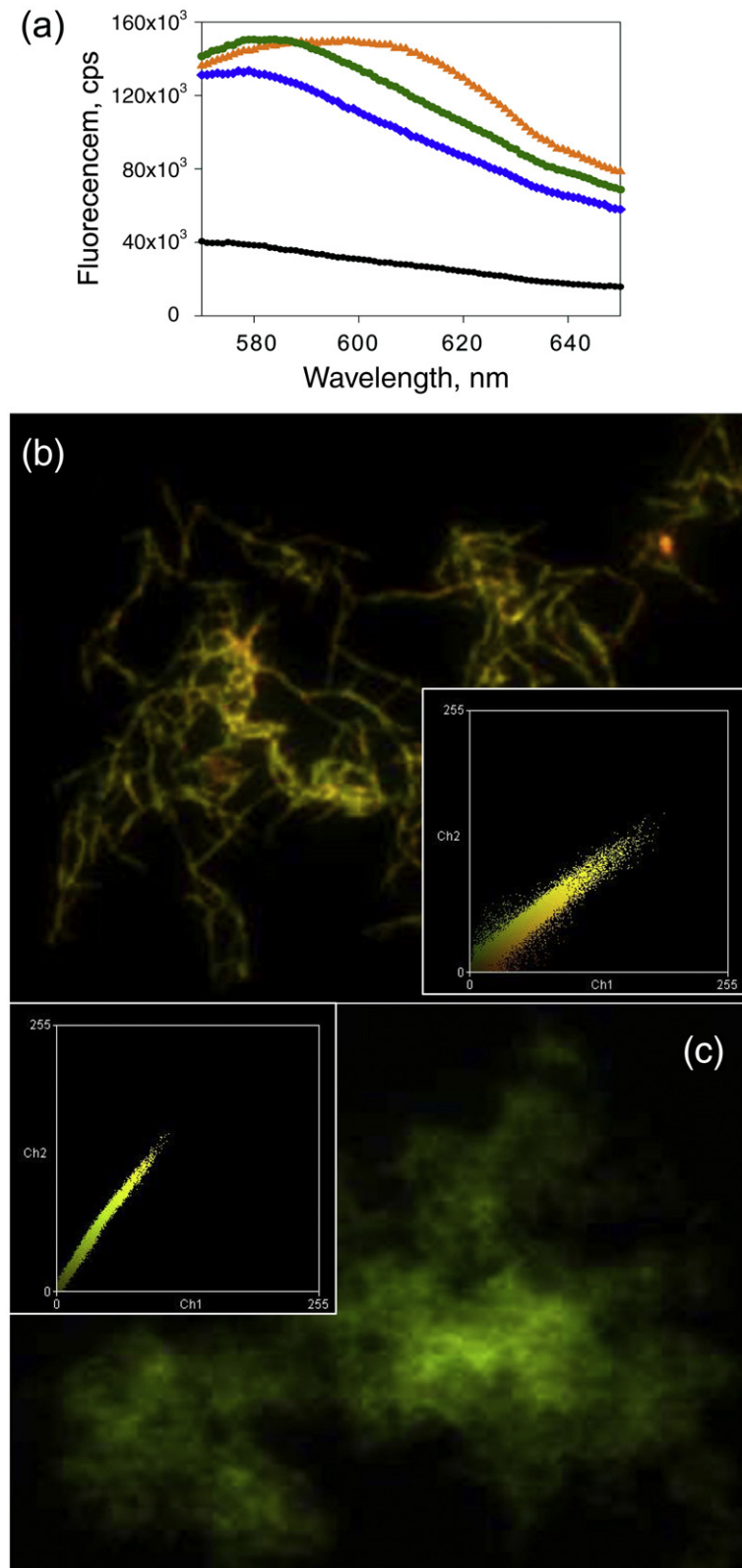
Fig. 5. Influence of R- and S-fibrils on PTAA fluorescence. (a) Fluorescence emission spectra of PTAA alone (black line) and PTAA in the presence of monomeric α-PrP (blue line), S-fibrils (green line), or R-fibrils (orange line) upon excitation at 540 nm. Fluorescence microscopy images of PTAA bound to R-fibrils (b) or to S-fibrils (c). The microscopy images were transformed into two-dimensional fluorescence intensity scattering plots (insets) as previously described.[25] Red fluorescence intensities are plotted on the horizontal axis, and the green fluorescence intensities are plotted on vertical axis. All PrP isoforms and PTAA were used at the concentrations 5 and 10 μg/ml, respectively, for both fluorescence spectroscopy and microscopy imaging.

Amyloid nature of prion fibrils

X-ray diffraction analysis confirmed cross-β-structures in both R- and S-fibrils with the meridional profile showing a single reflection at 4.8 Å. On the contrary, equatorial profiles of R- and S-fibrils displayed very distinctive sets of bands (Fig. 1). While lower-resolution reflections (corresponding to distances of >15 Å) presumably reflect filament dimensions,[26,27] reflections in the 8- to 15-Å range are believed to correspond to the distances between β-sheets in the dimensions perpendicular to the

fibril axis.[28,29] Notably, the pattern of equatorial reflections from the S-fibrils was very similar to the one reported recently for hamster PrP[Sc] (abnormal, disease-associated isoform of the prion protein) strain Sc237.[26] With slight deviation, both profiles contained bands at 7–8, 9.3, and 11 Å. The discrepancy between exact positions could possibly originate from higher-order diffraction of a very strong reflection at ∼60 Å in the case of Sc237. While many fibrils produced *in vitro* from amyloidogenic proteins are characterized by a single thick band at around 10 Å,[28] PrP R-fibrils showed two and S-fibrils
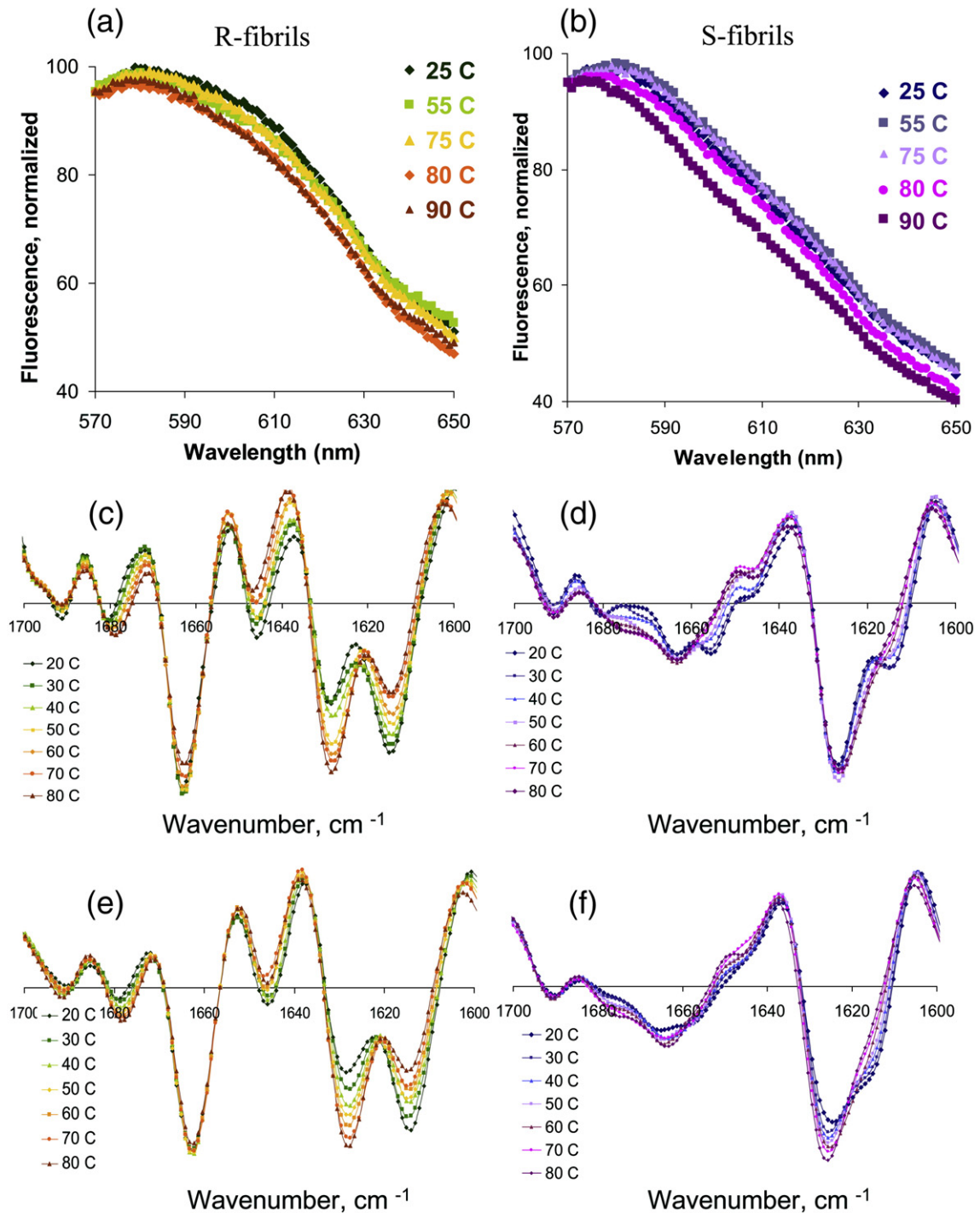
Fig. 6. The R-and S-fibrils were stable to thermal treatment as probed by PTAA fluorescence and FTIR spectroscopy. Fluorescence spectra of PTAA in the presence of R-fibrils (a) or S-fibrils (b). Prior to fluorescence measurements, fibrils were exposed to high temperatures as indicated, cooled down, and then mixed with PTAA. Second derivative of FTIR spectra for R-fibrils (c and e) or S-fibrils (d and f) recorded during the time course of heating from 20 to 80 °C (c and d) or cooling from 80 to 20 °C (e and f) at 10 °C intervals.

showed four distinctive bands within the same region. Overall, X-ray diffraction analysis revealed that the folding pattern of PrP molecules within R- and S-fibrils is clearly different.

Structural basis of amyloid states

Distinct prion strains have to be thermodynamically and kinetically stable to be able to propagate individual structures with high fidelity. Such high stability can be achieved if each individual amyloid state occupies a separate deep free-energy minima in a free-energy landscape and if these minima are separated by large energetic barriers.[7] To test this hypothesis, we measured the extent to which amyloid states are stable to thermal denaturation and whether they maintain their individual features during partial denaturation.

The experiments on thermal denaturation revealed that within the range of the tested temperatures (up to 80 °C), the S- and R-fibrils were equally stable. As judged from PTAA fluorescence and FTIR spectroscopy, both amyloid states maintained their individual features at the temperatures at which the monomeric α-PrP is known to be fully unfolded.[30,31] Furthermore, no signs of transition from R- to S-structure or vice versa were observed at high temperatures. With few exceptions including globular proteins from extremophiles, only cross-β-structures can resist such highly denaturing conditions. Furthermore, the local unfolding observed upon heating up to 80 °C was reversible, confirming that PrP molecules preserved their individual folds within their amyloid states even under partially denaturing conditions. These results strongly support the idea that state-specific features are encoded by different structures of cross-β-spines, that is, originate from distinctive folding and assembly patterns. These results also provide a molecular basis for explaining the high fidelity of replication of R- and S-fibrils, that is, their ability to maintain their individual structures during replication under unfavorable agitation conditions as was shown in our previous studies.[2]

Relationship between PrP^Sc and PrP fibrils

As judged from FTIR spectroscopy, the conformations of different PrP^Sc strains isolated from scrapie brains appear to have more common features[32–34] than the conformations of S- and R-fibrils generated *in vitro*. It is quite likely that posttranslational modifications with carbohydrates and the glycosylphosphatidylinositol anchor limit the conformational space occupied by different PrP^Sc strains in comparison to that of PrP fibrils generated in *vitro*.

In recent studies, we showed that the transmissible form of prion diseases can be induced in wild-type animals by inoculating annealed R-fibrils.[35] S-fibrils, on other hand, failed to induce the prion disease in wild-type animals.[35] These results are surprising considering substantial differences in global structures of R-fibrils and PrP^Sc. The data on

infectivity, however, support the previously introduced hypothesis that the R-structure is more promiscuous than the S-structure;[36,37] that is, it is capable of seeding the conversion of PrP^C (normal cellular isoform of the prion protein) into PrP^Sc despite the lack of compatibility between PrP^C and the structure of R-fibrils. Taken together, our studies suggest that only partial similarities or overlap in structures of R-fibrils and PrP^Sc was sufficient for seeding the conversion of PrP^C into PrP^Sc by R-structures.

Insight into cross-β-spine of amyloid states

The cross-β-spine is a key structural element of amyloid fibrils and as such represents a major target for developing anti-amyloid drugs.[38–40] We employed three different approaches including H/D exchange, FTIR spectroscopy combined with temperature denaturation, and a PK digestion assay to assess the differences in the β-spines of the two amyloid states of PrP.

While FTIR analysis might not reflect accurately the actual composition of secondary structure, nevertheless, this method is useful for comparing the structures of PrP amyloid states and PrP^Sc strains that were previously characterized by FTIR.[41,42] In FTIR spectra, both CB-1 and CB-2 bands report on cross-β-structure, where the latter is believed to represent more rigid β-sheets than the former. Notably, a similar double peak arising from cross-β-structure was found in FTIR spectra of PrP^Sc strains.[33,34] CB-2 was found to be significantly smaller in S-fibrils than in R-fibrils. Considering that the fraction of β-structure involved in the interfaces between filaments is greater in R- than in S-fibrils, this result suggests that CB-2 corresponds to the β-sheets that form an interface between filaments, whereas solvent-exposed β-sheets produce CB-1. Consistent with this idea, CB-2 was not influenced by H/D exchange but was substantially reduced upon heating when the filaments seem to dissociate apart. The inter-filament backbone–side chain and/or side chain–side chain hydrogen bonds could provide additional rigidity for the CB-2 β-sheets that form the interface between filaments.

As judged from FTIR, the percentage of β-sheet structures in R- and S-states (~44% and ~40%, respectively) were very similar to those previously found in the classical, PK-resistant form of PrP^Sc (~43%).[41,42] The length of the PK-resistant spine, however, was substantially smaller in R- and S-fibrils (~44% and ~55%, respectively, calculated per full-length PrP taken as 100%) than that in classical PrP^Sc (~70%). These results illustrate that (i) there is no direct correlation between the size of PK-resistant regions and the amount of β-structure and (ii) the PK-resistant regions can include protease-resistant folds other than cross β-sheet structure. Interestingly, exposure of PK-resistant PrP^Sc to the mild concentrations of denaturants was shown to expose additional cleavage sites at residues 139, 142, and 154.[43,44] Remarkably, these sites were very similar to the PK-

cleavage sites at residues 138/141 and 152/153 in R-fibrils, which, when cleaved, produce two C-terminal PK-resistant fragments of 10 and 12 kDa.[22,45] While the global folds of PrP[Sc] and *in vitro*-generated PrP fibrils appear to be different,[26] these results suggest that PrP[Sc] and PrP fibrils might share some common elements of secondary structure.

Because amyloid cross-β-spines are believed to be intrinsically stable to H/D exchange, this approach has been employed for assessing the size of the fibrillar β-sheet spine.[46,47] In the current study, the level of amide protection was found to be quite low for both states of PrP fibrils, approaching the level found in globular proteins. In part, such a low level of amide protection could be attributed to the fact that substantial portions of the polypeptide are not involved in forming cross-β-spine in PrP fibrils. However, the level of amide protection appears to be still substantially lower that one would expect considering that the proteolytically resistant regions encompassed ∼44% or ∼55% of residues in R- or S-fibrils, respectively, and that the cross-β-sheet content (by FTIR) was ∼44% or ∼40%, respectively. Therefore, the H/D exchange experiments argue that the PrP cross-β-structures are dynamic and capable of exchanging protons at reasonably high rates. In globular proteins, hydrogen exchange can result from various processes such as global or local unfolding or rapid structural fluctuations.[48,49] To explain fast hydrogen exchange and low fraction of amides protected in PrP fibrils, it is tempting to speculate that parts of PrP amyloid cross-β-spines might exhibit high propensity to undergo local unfolding or structural fluctuations.

Previous studies on solution NMR spectroscopy of Aβ amyloid demonstrated that the amide hydrogens of the inner β-strands that formed the interface between filaments were nearly 100% protected from exchange, whereas the amides in the outer solvent-exposed β-sheet layer showed only 50–80% protection.[50] In the current studies, the amides in R-fibrils showed a significantly higher level of protection than those in S-fibrils (∼15% *versus* ∼9% in "wet samples", respectively). The higher protection in R-fibrils was surprising considering that they had a smaller PK-resistant spine. Because of the differences in the fibril morphology and, specifically, complex multifilament twisting morphology in R-fibrils, a substantially larger surface area of β-sheets appears to be involved in forming the inter-filament interface in R-fibrils than in S-fibrils. Therefore, the level of amide protection correlates better with the complexity of fibril morphology, that is, with the fraction of surface area involved in the inter-filament interface than with the size of the PK-resistant spine.

Role of the N-terminal region in prion propagation

Because the unstructured N-terminal region was previously shown to be unessential for converting PrP[C] into PrP[Sc],[51,52] this region has frequently been ignored in previous studies. The current work illustrates that the N-terminal region forms part of the PK-resistant spine in S-fibrils and emphasizes the important role of this region for prion conversion. First, our study argues that the disordered N-terminus is capable of direct interaction with the C-terminal domain. This result is consistent with previous work on motif-grafted antibodies that showed high affinity of binding of PrP19–33 peptide to PrP[Sc].[53,54] Furthermore, our previous study on site-specific fluorescent labeling of PrP variants revealed direct involvement of the N-terminal region in the initial steps of *in vitro* fibril formation.[55] Second, even though the N-terminal region has never been found to be a part of the PK-resistant spine in authentic PrP[Sc], its involvement in forming a PK-resistant spine in the S-but not R-fibrils supports the idea that the N-terminus plays an active role in determining prion strain diversity. Third, the current studies provide a mechanistic explanation for our previous results that the presence of miniscule amounts of N-terminally truncated PrP polypeptide in a mixture with intact PrP poisons the fibrillation pathway that leads to S-fibrils.[30] As a part of the S-fibrillar spine, the N-terminus might be involved in forming an interface essential for elongation of S-fibrils; therefore, its deletion might block elongation of S-fibrils.

Conformation-sensitive LCPs

Two major parameters are believed to control LCP emission spectra upon their binding to the fibrillar surface: planarity and stacking of dye molecules. Twisted LCP chains were found to emit in green (∼530 nm), whereas a planar LCP backbone leads to gradual red shift in emission spectra.[23] Tight stacking of LCPs results in intermolecular energy transfer between LCP molecules causing further red shift in emission spectra to ∼640 nm. Therefore, LCP emission offers a valuable tool for assessing conformational properties of amyloids.

Significant red shift in PTAA emission spectra suggests that PTAA molecules are spaced much more tightly upon their binding to R-fibrils than to S-fibrils. The differences in charge distribution on the fibrillar surface could account in part for the differences in the density of PTAA stacking. In contrast to S-fibrils, the R-fibrils seem to expose the N-terminus to solvent, forming a positively charged matrix that favors dense stacking of polyanion PTAA. Considering that other polyanions were found to be crucially involved in formation of authentic PrP[Sc] *in vitro*,[56–58] PTAA could be very useful not only as a probe for detecting prion aggregates in a tissue but also as a sensitive polyanion-specific structural marker of prion strains.

In recent studies, the process of adaptation of CWD strains in mice was shown to be accompanied by a substantial red shift in PTAA emission spectra upon its binding to PrP[Sc] plaques.[23] We have previously suggested that the cross-species transmission of prions to new hosts should lead to an increase in conformational promiscuity of prion strains, that is, an increase in their ability to recruit heterologous

PrP^C molecules and/or expand the range of compatible heterologous PrP^C variants.[36,37] It would be interesting to determine in future studies whether the LCPs can be used as probes for conformational promiscuity of prion strains. The current work revealed that PTAA binding to R-fibrils is accompanied by a substantial red shift in its emission spectra relative to that of S-fibrils, supporting the idea that red shift in PTAA emissions correlates with the conformational promiscuity of an amyloid state. We previously showed that the R-conformation is highly promiscuous, as it preserves its individual properties within hamster, mouse, or even in a mixture of hamster and mouse PrPs,[59] whereas the S-conformation is strictly hamster-specific.[36]

Materials and Methods

Formation of fibrils from PrP

Recombinant full-length hamster PrP (residues 23–231, no tags) was expressed and purified as previously described.[30] To prepare fibrils for structural studies, we conducted the fibrillation reactions in 2 M Gdn–HCl and 50 mM 4-morpholineethanesulfonic acid, pH 6.0, at 37 °C at slow agitation (~60 rpm) and PrP concentration of 0.25 mg/ml for R-fibrils and at rapid shaking (~1000 rpm) and PrP concentration of 0.5 mg/ml for S-fibrils. The yield of conversion to fibrillar forms was estimated by SDS-PAGE as previously described[59] and was found to be >95% for each preparation. Identities of fibrils were confirmed by AFM and FTIR for each preparation used in the current study.

X-ray diffraction

The samples of R- or S-fibrils (500 μl of 2 mg/ml in 5 mM sodium acetate) were concentrated by placing them in separate centrifugal concentrators (Centricon, 10-kDa molecular mass cutoff) and spun at 5000 rpm for 1 h in an SS34 rotor. The concentrated samples were washed once with 2 ml water and further concentrated to a final volume of 20 μl in a Microcon concentrator (3-kDa molecular mass cutoff). The samples were viscous at this point. After 30 s of sonication in a water bath, they were diluted with 10 μl water. A volume of 5 μl of each sample was pipetted between the ends of two glass rods. The ends of the glass rods were fire polished and then scratched with fine sandpaper. The samples dried at room temperature for 8 h in a closed Petri dish, forming a fiber that stretched between the rods. Diffraction patterns were collected using a Rigaku FR-E X-ray generator with a Cu rotating anode equipped with a Rigaku HTC imaging plate detector. The samples were cooled to 100 K. Exposures were collected for 8 min. The crystal-to-film distance was 300 mm. Three independent measurements were performed for each sample.

FTIR spectroscopy, H/D exchange, and thermal denaturation

Infrared spectra were measured using a Bruker Tensor 27 FTIR instrument (Bruker Optics, Billerica, MA).

Samples were dialyzed for 4 h against 10 mM Na-acetate buffer, pH 5.0, with the buffer changed after 2 h. Fifteen microliters of sample was loaded into a BioATR II cell, and 512 scans were collected at 2 cm^{-1} resolution under constant purging with nitrogen. Spectra were corrected for the buffer and water vapors. Absorption bands were resolved by Fourier self-deconvolution using Lorentzian parameters of 20 cm^{-1} bandwidth and a noise suppression factor of 0.3. Second derivatives of deconvoluted spectra were calculated using either 9-point (for spectra interpolation with Lorentz curves) or 17-point (in other cases) Savitzky–Golay smoothing. To deconvolute the original absorbance spectra to individual peaks, the Opus manual fitting procedure (Opus 4.2 software package, Bruker Optics) was employed by setting the peak maxima at wavelengths taken from FTIR second derivative spectra. The minimal Euclidian distance between a spectrum and a fit was achieved by varying height and width of individual peaks.

For H/D exchange experiments, two formats were used. In the format referred to as "dried samples", the samples were dried off using Savant Speed Vac Concentrator (Thermo Scientific, Waltham, MA) and resolubilized in D$_2$O immediately before scanning in BioATR II cell. Thirty-two scans were collected for each time point during H/D exchange conducted for 5 h. Spectra of D$_2$O were collected under the same scanning conditions and at the same time points and subtracted from the sample spectra. In the format referred to as "wet samples", the samples were concentrated in Nanosep 100 K centrifuge tubes at 5000g for 2 min and D$_2$O was added up to the initial volume. This procedure was repeated 3 times to ensure D$_2$O content being >99%. Considering that the whole procedure for replacing H$_2$O to D$_2$O takes ~10 min, the 5 h of H/D exchange included 10 min of dead time. One hundred twenty-eight scans were collected for each sample. In both formats, H/D exchange was monitored for 5 h, the amide II-to-amide I ratio was calculated for each time point and normalized using FTIR spectra collected in H$_2$O.

For the thermal denaturation assay, the temperature in the BioATR II cell was controlled using a Haake K10 Refrigerated Circulator Bath (Thermo Scientific) operated with Opus/Protein software. Samples were heated from 20 to 80 °C by increasing the temperature in 10 °C increments over 15 min each and then cooled back to 20 °C in 10 °C decrements over 15 min each. One hundred twenty-eight scans were taken at each temperature step. Spectra were corrected for the buffer and water vapors, spectra of which were measured under the same scanning and temperature conditions.

CD spectroscopy

CD spectra of PrP isoforms (~0.25 mg/ml) were recorded in 5 mM sodium acetate buffer, pH 5.0, in a 0. 1-cm cuvette with a J-810 CD Spectrometer (Jasco Inc., Easton, MD) at 50 nm/min scanning rate and resolution of 1 nm. Each spectrum represents the average of five individual scans after subtracting the background spectrum of the buffer. CD spectra were recorded for three independent preparations of R- or S-fibrils and were found to be identical for the same fibrillar types. For the sake of clarity, repeated spectra were omitted from the figures. To prepare sonicated fibrils, we sonicated R- or S-fibrils for 1 min in a bath sonicator Bransonic-2510 as previously described,[60] and their spectra were collected under the same conditions.

PK digestion assay

PK digestion was performed in a reaction volume of 20 μl containing 100 μg/ml of fibrils and varying concentrations of PK (from 0.2 to 50 μg/ml) in 0.1 M Tris–HCl buffer, pH 7.5, for 1 h at 37 °C. Reactions were quenched with 1 mM PMSF and then samples were treated with the sample buffer (2% SDS, 1.25% β-mercaptoethanol, and 2.25 M urea, heating for 15 min at 90 °C) and analyzed using 12% SDS-PAGE (precast NuPAGE gels, Invitrogen) followed by silver staining. For N-terminal sequencing, PK-resistant fragments were transferred from SDS-PAGE to polyvinylidene fluoride membrane, stained with Coomassie R-250, and analyzed at the Tufts University Core Facility (Boston, MA).

Fluorescent microscopy and spectroscopy

PTAA was synthesized as previously described.[61] PrP fibrils (or monomers) and PTAA were mixed to final concentrations 5 and ~10 μg/ml, respectively, in 5 mM Hepes buffer, pH 7.0, and deposited on a cover glass (Fisher Scientific, Pittsburgh, PA). Fluorescence images were recorded using an inverted microscope Eclipse TE2000 (Nikon, Japan) with a 1.3 aperture Plan Fluor 100× with numerical aperture objective and two sets of filters: (i) Chroma 49002 ET-GFP (fluorescein isothiocyanate/Cy2) for a green channel (excitation, 470 ± 20 nm; emission, 525 ± 25 nm) and (ii) Chroma 41006 Eth Bro for a red channel (excitation, 535 ± 25 nm; emission, 610 ± 30 nm). Images collected in the two channels were processed with WCIF ImageJ software (National Institutes of Health, Bethesda, MD). Fluorescence emission spectra were recorded using FluoroMax-3 spectrofluorimeter (HORIBA Jobin Yvon Inc., Edison, NJ) with an excitation at 540 nm. Each spectrum represents the average of five individual scans.

For the thermal denaturation assay, PrP fibrils in 5 mM sodium acetate buffer, pH 5.0, were heated from 20 to 95 °C with a rate of 1 °C/min in PC-controlled RTE-111 Neslab thermostat. Aliquots were taken at 5 °C increments, diluted with 5 mM Hepes buffer, pH 7.0, to a final PrP concentration of 5 μg/ml, incubated at room temperature for 30 min, and mixed with PTAA at a final concentration of 10 μg/ml. Emission spectra were measured as described above.

Atomic force microscopy

AFM imaging was performed using Pico LE system (Agilent Technologies, Chandler, AZ) operated in the acoustic alternative current mode using a silicon cantilever PPP-NCH (Nanosensors, Switzerland) at the resonant frequency $f_0 \sim 300$ kHz. The AFM scanner was operated in tapping mode. The images (512×512 pixels) were collected at a scan rate of one line per second. To analyze the products of fibrillation reactions, we dialyzed samples in 10 mM sodium acetate buffer, pH 5.0, for 4 h, changing the buffer after 2 h. Ten microliters of a sample (PrP concentration, 20 μg/ml) was applied on a freshly cleaved piece of mica, incubated for 5 min at room temperature to adhere, washed by Milli-Q water, and dried at room temperature.

Acknowledgements

Supplementary Data

Supplementary data associated with this article can be found, in the online version, at doi:10.1016/j.jmb.2010.05.051

References

1. Petkova, A. T., Leapman, R. D., Gua, Z., Yau, W.-M., Mattson, M. P. & Tycko, R. (2005). Self-propagating, molecular-level polymorphism in Alzheimer's β-amyloid fibrils. *Science*, **307**, 262–265.
2. Makarava, N. & Baskakov, I. V. (2008). The same primary structure of the prion protein yields two distinct self-propagating states. *J. Biol. Chem.* **283**, 15988–15996.
3. Tanaka, M., Chien, P., Naber, N., Cooke, R. & Weissman, J. S. (2004). Conformational variations in an infectious protein determine prion strain differences. *Nature*, **6980**, 323–328.
4. Krishnan, R. & Lindquist, S. (2005). Structural insights into a yeast prion illuminate nucleation and strain diversity. *Nature*, **435**, 765–772.
5. Wiltzius, J. J. W., Landau, M., Nelson, R., Sawaya, M. R., Apostol, M. I., Goldschmidt, L. *et al.* (2009). Molecular mechanisms for protein-encoded inheritance. *Nat. Struct. Mol. Biol.* **16**, 973–978.
6. Prusiner, S. B. (1998). Prions. *Proc. Natl Acad. Sci. USA*, **95**, 13363–13383.
7. Dzwolak, W., Grudzielanek, S., Smirnovas, S., Ravindra, R., Nicolini, C., Jansen, R. *et al.* (2005). Ethanol-perturbed amyloidogenic self-assembly of insulin: looking for origins of amyloid strains. *Biochemistry*, **44**, 8948–8958.
8. Pedersen, J. S., Dikov, D., Flink, J. L., Hjuler, H. A., Christiansen, G. & Otzen, D. E. (2006). The changing face of glucagon fibrillation: structural polymorphism and conformational imprinting. *J. Mol. Biol.* **355**, 501–523.
9. Frost, B., Ollesch, J., Wille, H. & Diamond, M. I. (2009). Conformational diversity of wild-type Tau fibrils specified by templated conformation change. *J. Biol. Chem.* **284**, 3546–3551.
10. Paravastu, A. K., Leapman, R. D., Yau, W. M. & Tycko, R. (2008). Molecular structural basis for polymorphism in Alzheimer's beta-amyloid fibrils. *Proc. Acad. Natl Sci. USA*, **105**, 18349–18354.
11. Sawaya, M. R., Sambashivan, S., Nelson, R., Ivanova, M. I., Sievers, S. A., Apostol, M. I. *et al.* (2007). Atomic structures of amyloid cross-beta spines reveal varied steric zippers. *Nature*, **447**, 453–457.
12. Jimenez, J. L., Nettleton, E. J., Bouchard, M., Robinson, C. V., Dobson, C. M. & Saibil, H. (2002). The protofilament structure of insulin amyloid fibrils. *Proc. Acad. Natl Sci. USA*, **99**, 9196–9201.
13. Gosal, W. S., Morten, I. J., Hewitt, E. W., Smith, D. A., Thompson, N. H. & Radford, S. E. (2005). Competing pathways determine fibril morphology in the self-assembly of beta-microglobulin into amyloid. *J. Mol. Biol.* **351**, 850–864.
14. Diaz-Avalos, R., King, C. Y., Wall, J., Simon, M. & Caspar, D. L. D. (2005). Strain-specific morphologies

of yeast prion amyloid fibrils. *Proc. Acad. Natl Sci. USA*, **102**, 10165–10170.

15. Goldsbury, C., Frey, P., Olivieri, V., Aebi, U. & Muller, S. A. (2005). Multiple assembly pathways underlie amyloid-b fibril polymorphysms. *J. Mol. Biol.* **352**, 282–298.

16. Anderson, M., Bocharova, O. V., Makarava, N., Breydo, L., Salnikov, V. V. & Baskakov, I. V. (2006). Polymorphism and ultrastructural organization of prion protein amyloid fibrils: an insight from high resolution atomic force microscopy. *J. Mol. Biol.* **358**, 580–596.

17. Makarava, N., Bocharova, O. V., Salnikov, V. V., Breydo, L., Anderson, M. & Baskakov, I. V. (2006). Dichotomous versus palm-type mechanisms of lateral assembly of amyloid fibrils. *Protein Sci.* **15**, 1334–1341.

18. Sim, V. L. & Caughey, B. (2009). Ultrastructures and strain comparison of under-glycosylation scrapie prion fibrils. *Neurobiol. Aging*, **30**, 2031–2042.

19. Liberski, P. P., Brown, P., Xiao, S.-Y. & Gajdusek, D. C. (1991). The ultrastructural diversity of scrapie-associated fibrils isolated from experimental scrapie and Creutzfeldt–Jakob disease. *J. Comp. Pathol.* **105**, 377–386.

20. Krimm, S. & Bandekar, J. (1986). Vibrational spectroscopy and conformation of peptides, polypeptides, and proteins. *Adv. Protein Chem.* **38**, 297–328.

21. Perczel, A. & Fasman, G. D. (1992). Quantitative analysis of cyclic beta-turn models. *Protein Sci.* **1**, 378–395.

22. Bocharova, O. V., Breydo, L., Salnikov, V. V., Gill, A. C. & Baskakov, I. V. (2005). Synthetic prions generated *in vitro* are similar to a newly identified subpopulation of PrPSc from sporadic Creutzfeldt–Jakob Disease PrP^Sc. *Protein Sci.* **14**, 1222–1232.

23. Sigurdson, C. J., Nilsson, K. P. R., Hornemann, S., Manco, G., Polymenidou, M., Schwarz, P. *et al.* (2007). Prion strain discrimination using luminescent conjugated polymers. *Nat. Methods*, **4**, 1023–1030.

24. Almstedt, K., Nyström, S., Nilsson, K. P. R. & Hammarström, P. (2009). Amyloid fibrils of human prion protein are spun and woven from morphologically disordered aggregates. *Prion*, **3**, 224–235.

25. Novitskaya, V., Makarava, N., Bellon, A., Bocharova, O. V., Bronstein, I. B., Williamson, R. A. & Baskakov, I. V. (2006). Probing the conformation of the prion protein within a single amyloid fibril using a novel immunoconformational assay. *J. Biol. Chem.* **281**, 15536–15545.

26. Wille, H., Bian, W., McDonald, M., Kendall, A., Colby, D. W., Bloch, L. *et al.* (2009). Natural and synthetic prion structure from X-ray fiber diffraction. *Proc. Acad. Natl Sci. USA*, **106**, 16990–16995.

27. Malinchik, S. B., Inouye, H., Szumowski, K. E. & Kirschner, D. A. (1998). Structural analysis of Alzheimer's (1–40) amyloid: protofilament assembly of tubular fibrils. *Biophys. J.* **74**, 537–545.

28. Sunde, M., Serpell, L. C., Bartlam, M., Fraser, P. E., Pepys, M. B. & Blake, C. C. (1997). Common core structure of amyloid fibrils by synchrotron X-ray diffraction. *J. Mol. Biol.* **273**, 729–739.

29. Jahn, T. R., Makin, O. S., Morris, K. L., Marshall, K. E., Tian, P., Sikorski, P. & Serpell, L. C. (2010). The common architecture of cross-beta amyloid. *J. Mol. Biol.* **395**, 717–727.

30. Ostapchenko, V. G., Makarava, N., Savtchenko, R. & Baskakov, I. V. (2008). The polybasic N-terminal region of the prion protein controls the physical properties of both the cellular and fibrillar forms of PrP. *J. Mol. Biol.* **383**, 1210–1224.

31. Nandi, P. K., Leclerc, E. & Marc, D. (2002). Unusual property of prion protein unfolding in neutral salt solution. *Biochemistry*, **41**, 11017–11024.

32. Caughey, B., Raymond, G. J. & Bessen, R. A. (1998). Strain-dependent differences in β-sheet conformations of abnormal prion protein. *J. Biol. Chem.* **273**, 32230–32235.

33. Thomzig, A., Spassov, S., Friedrich, M., Naumann, D. & Beekes, M. (2004). Discriminating scrapie and bovine spongiform encephalopathy isolates by Infrared spectroscopy of pathological prion protein. *J. Biol. Chem.* **279**, 33854.

34. Spassov, S., Beekes, M. & Naumann, D. (2006). Structural differences between TSEs strains investigated by FT-IR spectroscopy. *Biochim. Biophys. Acta*, **1760**, 1138–1149.

35. Makarava, N., Kovacs, G. G., Bocharova, O. V., Savtchenko, R., Alexeeva, I., Budka, H. *et al.* (2010). Recombinant prion protein induces a new transmissible prion disease in wild type animals. *Acta Neuropathol.* **119**, 177–187.

36. Makarava, N., Ostapchenko, V. G., Savtchenko, R. & Baskakov, I. V. (2009). Conformational switching within individual amyloid fibrils. *J. Biol. Chem.* **284**, 14386–14395.

37. Baskakov, I. V. (2009). Switching in amyloid structure within individual fibrils: implication for strain adaptation, species barrier and strain classification. *FEBS Lett.* **583**, 2618–2622.

38. Chen, Z., Krause, G. & Reif, B. (2005). Structure and orientation of peptide inhibitors bound to beta-amyloid fibrils. *J. Mol. Biol.* **354**, 760–767.

39. Chalifour, R. J., McLaughlin, R. W., Lavoie, L., Morissette, C., Tremblay, N., Boulé, M. *et al.* (2003). Stereoselective interactions of peptide inhibitors with the beta-amyloid peptide. *J. Biol. Chem.* **278**, 34874–34881.

40. Esteras-Chopo, A., Pastor, M. T., Serrano, L. & Lopez de la Paz, M. (2008). New strategy for the generation of specific D-peptide amyloid inhibitors. *J. Mol. Biol.* **377**, 1372–1381.

41. Pan, K.-M., Baldwin, M., Nguyen, J., Gasset, M., Serban, A., Groth, D. *et al.* (1993). Conversion of α-helices into β-sheets features in the formation of the scrapie prion proteins. *Proc. Natl Acad. Sci. USA*, **90**, 10962–10966.

42. Gasset, M., Baldwin, M. A., Fletterick, R. J. & Prusiner, S. B. (1993). Perturbation of the secondary structure of the scrapie prion protein under conditions that alter infectivity. *Proc. Natl Acad. Sci. USA*, **90**, 1–5.

43. Kocisko, D. A., Lansbury, P. T., Jr. & Caughey, B. (1996). Partial unfolding and refolding of scrapie-associated prion protein: evidence for a critical 16-kDa C-terminal domain. *Biochemistry*, **35**, 13434–13442.

44. Sajnani, G., Pastrana, M. A., Dynin, I., Onisko, B. & Requena, J. R. (2008). Scrapie prion protein structural constraints obtained by limited proteolysis and mass spectrometry. *J. Mol. Biol.* **382**, 88–98.

45. Bocharova, O. V., Makarava, N., Breydo, L., Anderson, M., Salnikov, V. V. & Baskakov, I. V. (2006). Annealing PrP amyloid fibrils at high temperature results in extension of a proteinase K resistant core. *J. Biol. Chem.* **281**, 2373–2379.

46. Dzwolak, W., Loksztejn, A. & Smirnovas, V. (2006). New insights into the self-assembly of insulin amyloid fibrils: an H–D exchange FT-IR study. *Biochemistry*, **45**, 8143–8151.

47. Chatani, E. & Goto, Y. (2005). Structural stability of amyloid fibrils of beta(2)-microglobulin in

comparison with its native fold. *Biochim. Biophys. Acta*, **1753**, 64–75.

48. Englander, S. W., Mayne, L., Bai, Y. & Sosnick, T. R. (1997). Hydrogen exchange: the modern legacy of Linderstrom–Lang. *Protein Sci.* **6**, 1101–1109.

49. Chung, E. W., Nettleton, E. J., Morgan, C. J., Gross, M., Miranker, A., Radford, S. E. *et al.* (1997). Hydrogen exchange properties of proteins in native and denatured states monitored by mass spectrometry and NMR. *Protein Sci.* **6**, 1316–1324.

50. Olofsson, A., Sauer-Eriksson, A. E. & Ohman, A. (2006). The solvent protection of Alzheimer amyloid-beta-(1–42) fibrils as determined by solution NMR spectroscopy. *J. Biol. Chem.* **281**, 477–483.

51. Flechsig, E., Shmerling, D., Hegyi, I., Raeber, A. J., Fischer, M., Cozzio, A. *et al.* (2000). Prion protein devoid of the octapeptide repeat region restores susceptibility to scrapie in PrP knockout mice. *Neuron*, **27**, 399–408.

52. Rogers, M., Yehiely, F., Scott, M. & Prusiner, S. B. (1993). Conversion of truncated and elongated prion proteins into the scrapie isoform in cultured cells. *Proc. Natl Acad. Sci. USA*, **90**, 3182–3186.

53. Moroncini, G., Kanu, N., Solforosi, L., Abalos, G., Telling, G. C., Head, M. *et al.* (2004). Motif-grafted antibodies containing the replicative interface of cellular PrP are specific for PrPSc. *Proc. Acad. Natl Sci. USA*, **101**, 10404–10409.

54. Solforosi, L., Bellon, A. B., Schaller, M., Cruite, J. T., Abalos, G. C. & Williamson, R. A. (2007). Toward molecular dissection of PrPC–PrPSc interactions. *J. Biol. Chem.* **282**, 7465–7471.

55. Sun, Y., Breydo, L., Makarava, N., Yang, Q., Bocharova, O. V. & Baskakov, I. V. (2007). Site-specific conformational studies of PrP amyloid fibrils revealed two cooperative folding domain within amyloid structure. *J. Biol. Chem.* **282**, 9090–9097.

56. Deleault, N. R., Harris, B. T., Rees, J. R. & Supattapone, S. (2007). Formation of native prions from minimal components in vitro. *Proc. Acad. Natl Sci. USA*, **104**, 9741–9746.

57. Deleault, N. R., Lucassen, R. W. & Supattapone, S. (2003). RNA molecules stimulate prion protein conversion. *Nature*, **425**, 717–720.

58. Ceoghegan, J. C., Valdes, P. A., Orem, N. R., Deleault, N. R., Williamson, R. A., Harris, B. T. & Supattapone, S. (2007). Selective incorporation of polyanionic molecules into hamster prions. *J. Biol. Chem.* **282**, 36341–36353.

59. Makarava, N., Lee, C. I., Ostapchenko, V. G. & Baskakov, I. V. (2007). Highly promiscuous nature of prion polymerization. *J. Biol. Chem.* **282**, 36704–36713.

60. Sun, Y., Makarava, N., Lee, C. I., Laksanalamai, P., Robb, F. T. & Baskakov, I. V. (2008). Conformational stability of PrP amyloid firbils controls their smallest possible fragment size. *J. Mol. Biol.* **376**, 1155–1167.

61. Ding, L., Jonforsen, M., Roman, L. S., Andersson, M. R. & Inganäs, O. (2000). Photovoltaic cells with a conjugated polyelectrolyte. *Synth. Met.* **110**, 133–140.